

Article

Rare Earth Elements in the Shok-Karagay Ore Fields (Syrymbet Ore District, Northern Kazakhstan) and Visualisation of the Deposits Using the Geography Information System

Kuanyshtogizov¹ , Lyudmila Issayeva² , Daulet Muratkhanov² , Madina Kurmangazhina² , Maciej Swęd³ and Agata Duczmal-Czernikiewicz^{4,*} 

¹ Department of Geophysics and Seismology, Satbayev University, Almaty 050013, Kazakhstan; k.togizov@satbayev.university

² Institute of Geological Sciences Named after K.I. Satpaev, Satbayev University, Almaty 050010, Kazakhstan; l.issayeva@satbayev.university (L.I.); daulet.muratkhonov@satbayev.university (D.M.); m.kurmangazhina@satbayev.university (M.K.)

³ Institute of Geological Sciences, Polish Academy of Science, 00-818 Warszawa, Poland; maciej.swed@twarda.pan.pl

⁴ Institute of Geology, Adam Mickiewicz University in Poznan, 61-686 Poznan, Poland

* Correspondence: duczer@amu.edu.pl

Abstract: Rare earth elements deposited in ion-adsorption clay-type deposits in Northern Kazakhstan were recognised using mineralogical and geochemical methods. The diversity and mineralogical properties of the Shok-Karagay deposit and Syrymbet ore fields under investigation in this study are closely related to the process of the formation of the deposits as well as the deposits' architecture. A combination of mineralogical research and digital technology (GIS) was used to characterise the deposits. Rare earth elements from the cerium series were found in the following quantities: La (in ppm), 43–200; Ce, 57–206; Sm, 100–300; Eu, 22–100. Yttrium-series elements were found in the following quantities: Y, 31–106; Gd, 100–200; Tb, 100–200; Dy, 0–300; Ho, 0–20; Er, 0–364; Tm, 0.28–0.85; Yb, 2.2–39; Lu, 0–200. The wireframe and block models indicated that the bodies' forms were 1800 m wide, 3500 m long, and 20–40 m thick. The major REE group minerals in both bodies were monazite and xenotime, whereas the minor minerals included yttrium parisite, silicorabdophanite, thorite, and orangite; moreover, ilmenite and titanomagnetite were found. The 3D models that were constructed indicated that the mineralogy and geochemistry of the ore bodies played a determining role in the deposits' architecture.

Keywords: rare earth elements; accessory minerals; ion-adsorption deposit; GIS models; Shok-Karagay; Kazakhstan



Citation: Togizov, K.; Issayeva, L.; Muratkhanov, D.; Kurmangazhina, M.; Swęd, M.; Duczmal-Czernikiewicz, A. Rare Earth Elements in the Shok-Karagay Ore Fields (Syrymbet Ore District, Northern Kazakhstan) and Visualisation of the Deposits Using the Geography Information System. *Minerals* **2023**, *13*, 1458. <https://doi.org/10.3390/min13111458>

Academic Editor: Paul Alexandre

Received: 29 September 2023

Revised: 3 November 2023

Accepted: 10 November 2023

Published: 20 November 2023



Copyright: © 2023 by the authors. Licensee MDPI, Basel, Switzerland. This article is an open access article distributed under the terms and conditions of the Creative Commons Attribution (CC BY) license (<https://creativecommons.org/licenses/by/4.0/>).

1. Introduction

The term rare earth elements (REEs) refers to elements from the lanthanide group in the periodic table. Yttrium (Y) and scandium (Sc) are regarded as REEs due to their similar chemical properties to lanthanide elements. Lanthanides are divided into the cerium series, commonly referred to as light rare earth elements (LREEs), and the yttrium series, which are referred to as heavy rare earth elements (HREEs). Rare earth elements play a vital role in the global economy because of their broad application in new energy technologies, electronic devices, automobiles, and national security. Therefore, the exploration and exploitation of REE deposits have been widely developed over the decades [1,2].

Rare earth elements are hosted in various deposit types that are formed through primary and secondary geological processes. The primary processes include magmatic, hydrothermal, and/or metamorphic processes, whereas the secondary processes include weathering and the transport of sediments. In relation to these terms, REE deposits are divided into primary and secondary deposits [3]. Primary REE deposits include

carbonatite-, alkaline-/peralkaline-, phosphorite-, and IOCG-related deposits. Secondary deposits, such as placers, bauxites, and weathering-related deposits, are formed through low-temperature processes: the erosion and weathering of primary deposits [3,4]. In 2016, the total global reserve of rare earth oxides (REOs) was estimated to be 120 Mt [5]. China reported approximately 4.4 Mt in 2021 [4,5]. Ion-adsorption deposits (IADs) are a type of REE deposit that were first discovered in 1969 in Southern China's Jiangxi Province as weathered crust-elution deposits with REE enrichments. They were later found in other Chinese provinces: Fujian, Hunan, Guangdong, and Guanxi [3,4,6]. Since the early 1970s, these deposits, generally 8–10 m thick, have been recognised as being enriched in HREEs, and they are considered easily recoverable resources [7,8]. Many prospective weathering profiles, some of which are HREE-enriched, have been studied outside China, including those in Kazakhstan [9,10], Malawi [11], Madagascar, the USA, Brazil, the Philippines, Laos, Thailand, and Myanmar [3].

The known reserve of these deposits contains more than 1×10^6 tons of REOs [6], but the ore grades contain substantially lower rare earth amounts, ranging from 0.05% to 0.2% REOs [6]. Despite their low grades, the extraction of REEs from these clay deposits is economically attractive due to their easy extractability [3]. Although these deposits account for only 0.97% of China's total REE resources, almost 35% of China's total REE production has come from this deposit type since 2009 [3,5]. Furthermore, this type of deposit accounts for more than 80% of global HREE resources and 70% of the world's production [4].

The Shok-Karagay regolith-hosted IAD REE deposit has become an important subject of recent studies [9,10]. It has large resources of REEs hosted in ionic clays, complex rare metal and rare earth mineralisation, and relatively low mining and processing costs based on ion exchange with a dilute electrolyte solution [11]. Moreover, digital scientific information databases are widely used for studying mineral deposits [12–15]. Digital databases have been successfully used in global practice to study ore elements' placement patterns and refine forecasting and search criteria [16–19].

The Shok-Karagay rare earth element deposit (northern Kazakhstan), located within the Syrymbet ore cluster (Figure 1), is characterised by rare metal and rare earth mineralisation. The Shok-Karagay deposit was discovered in 1961 during deep prospecting for uranium in the Syrymbet deposit area. Two sites containing rare earth elements were identified: Shok-Karagay South and Shok-Karagay North. The deposit accumulated in the weathering crusts of the upper Oligocene sediments, and the main share of the deposit's REEs is hosted in clays. At Shok-Karagay's south site, the cumulative content of REEs is in the range of 0.1–0.6 wt.%; approximately 20% of the yttrium is at Shok-Karagay's north site, and the sum of the rare earth elements' content ranges from 0.1 to 0.4% (the maximum is 0.8 wt.%) [19,20]. Although residual REE clays likely constitute >80% of the world's economic HREE resources [3], in the Shok-Karagay deposit, LREEs predominate among the rare earth elements. The deposit is economically attractive due to its association with clays.

A two-track approach was applied to our study: a description of the mineralogical features and the digital modelling of the deposit architecture based on the REE ores' geochemistry. The main objectives of this work were (1) to determine the mineral diversity in the Shok-Karagay rare earth deposit; (2) to determine the distribution of rare earth elements; (3) to visualise the 3D ore body architecture and percental distribution of rare earth elements in the Shok-Karagay deposit; and (4) to highlight the promising areas within its limits based on GIS technology. Moreover, with growing global demand for ion-adsorption-type REE deposits, it is important to better understand REE concentration regularities in the Shok-Karagay ore field, particularly due to the mineralogy and geochemistry of accessory minerals occurring in Shok-Karagay compared with other REE deposits in northern Kazakhstan.

2. Materials and Methods

We investigated a rare earth deposit located in the central part of the Shok-Karagay massif, representing a volcanic complex of granite porphyries and granophyres in its central

parts, with the margins comprising acidic volcanoclastic rocks (Figure 1) [20–22]. The massif is cut by dikes of felsite porphyries from the second phase of the Yakshi-Yangiztau complex, associated with mineralisation in the bedrock. The Shok-Karagay deposit area is cut by major multi-seam faults oriented to the northeast and minor faults with northwestern, submeridional, and sublatitudinal orientations (Figure 1). Felsite porphyry dikes are located in tectonic discontinuity zones resulting from processes of cataclases and crushing accompanied by different post-magmatic alterations, including potassium metasomatism and hematite and fluorite formation [22]. According to ground-based geophysical surveys, the rare-earth-bearing areas are delineated by local positive values of magnetic anomalies up to 400 nT and associated with granitoids of a subvolcanic type in both cases [9,20].

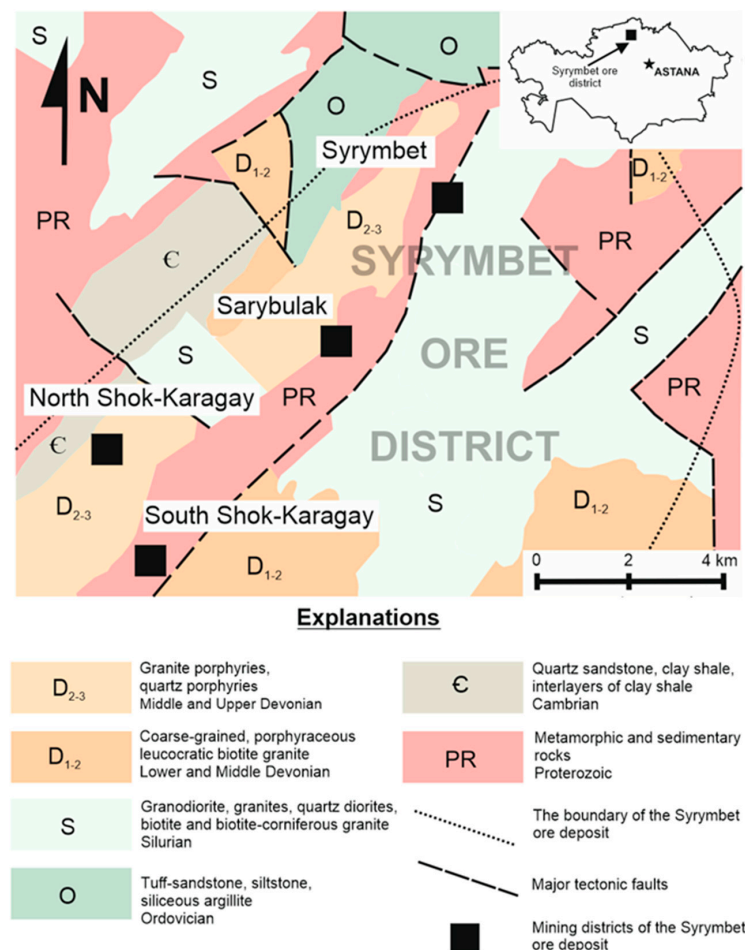


Figure 1. Geology of the Syrymbet ore field (simplified). PR—Zerendy series: gneiss, amphibolites, and crystalline schist; Sharyk suite: carbonaceous–clayey, siliceous–argillaceous slate, sandstone, limestone, interbedding quartzite, quartz sandstones, siltstones, and limestone lenses; Cm—Andreev suite: quartz sandstone, clay shale, and interlayers of clay shale; O—tuff–sandstone, siltstone, and siliceous argillite; S—granodiorite, granites, quartz diorites, biotite, and biotite–corniferous granite; D1–2—coarse-grained, sometimes porphyreous leucocratic biotite granite; D2–3—granite porphyries and quartz porphyries [23].

Materials for the mineralogical study were obtained from drill holes in the Shok-Karagay deposit area from 2012 to 2013. The samples were divided into heavy and light fractions (eight drill wells) by means of heavy fraction analyses. The wells were set along the strike of known ore bodies (Figure 2) to determine the possibility of their extension.



Figure 2. Location of exploration wells (points 7001–7007) overlaid on a geological map of the Shok-Karagay deposit. Scale: 1:25,000. Schemes follow the same formatting (Google Maps) [23]. Red lines: cross-sections. Yellow stars: sampling points.

2.1. Mineralogy and Geochemistry

The mineral and chemical composition was studied at the mineralogical laboratory of the Institute of Geological Sciences in Almaty. MBS-9, a binocular stereoscopic microscope, was used to research the weathering crusts' mineral composition. The magnification ranged from $3.3\times$ to $100\times$, and the linear field of view was from 39 to 2.4 mm. The working distance was 64 mm. The light source for studying petrography in the polished section was an MBS-9 halogen lamp.

To obtain the chemical composition and REE content of the studied ores, atomic spectral analyses (ASAs) were used. A semiquantitative atomic spectral analysis (ASA) was performed on a DFS-3 diffraction spectrograph with a diffraction grating of 500 lines per mm. The inverse linear dispersion of the device was 0.4 nm/mm. The resolving power of the spectrograph was approximate to the theoretical one, reaching 720,000. An electric arc of 14 amperes was used as a source of spectra emissions. The spectra were photographed on PFS-03 photographic plates in the spectrum's ultraviolet region in a wavelength range from 230 to 346 nm.

Mineralogical observations on a microscale of the selected heavy minerals were obtained using a scanning electron microscope (SEM), and the semiquantitative chemical composition of the minerals was studied using energy-dispersive spectroscopy (EDS) (model Hitachi S-3700N) at the Faculty of Geographical and Geological Sciences of the Adam Mickiewicz University in Poznań. The chemical composition on the microscale was studied by means of an electron microprobe analysis using JXA 733 equipment and an INCA ENERGY energy-dispersive spectrometer at an accelerating voltage of 15 kV and a 25 nA probe current with a focused (1–2 μm diameter) probe.

X-ray phase analysis was conducted using a DRON-3 diffractometer with CuK α radiation (β -filter). The measurement parameters were: $U = 35$ kV; $I = 20$ mA; θ – 2θ geometry; and a detector step of $2^\circ/\text{min}$. An X-ray semiquantitative phase analysis of powdered samples was performed. Interpretation of the diffraction patterns was conducted using the ICDD (International Centre for Diffraction Data): base powder diffractometric PDF2 (powder diffraction file) data and the diffraction patterns of pure (free from impurities) minerals.

2.2. GIS Technology

This study includes the construction of digital models of the deposit, visualising the forms of ore bodies in three-dimensional space and their ore element contents; the systematisation of ore-controlling factors specifying the prognostic and prospecting criteria; and the allocation of promising areas in the deposit site. Constructing the 3D geological models and compiling the digital field database required the use of cartographic materials, geological maps and sections, and the spectral analysis results for all the collected samples (well Nos. 7001–7008) (Figure 3).

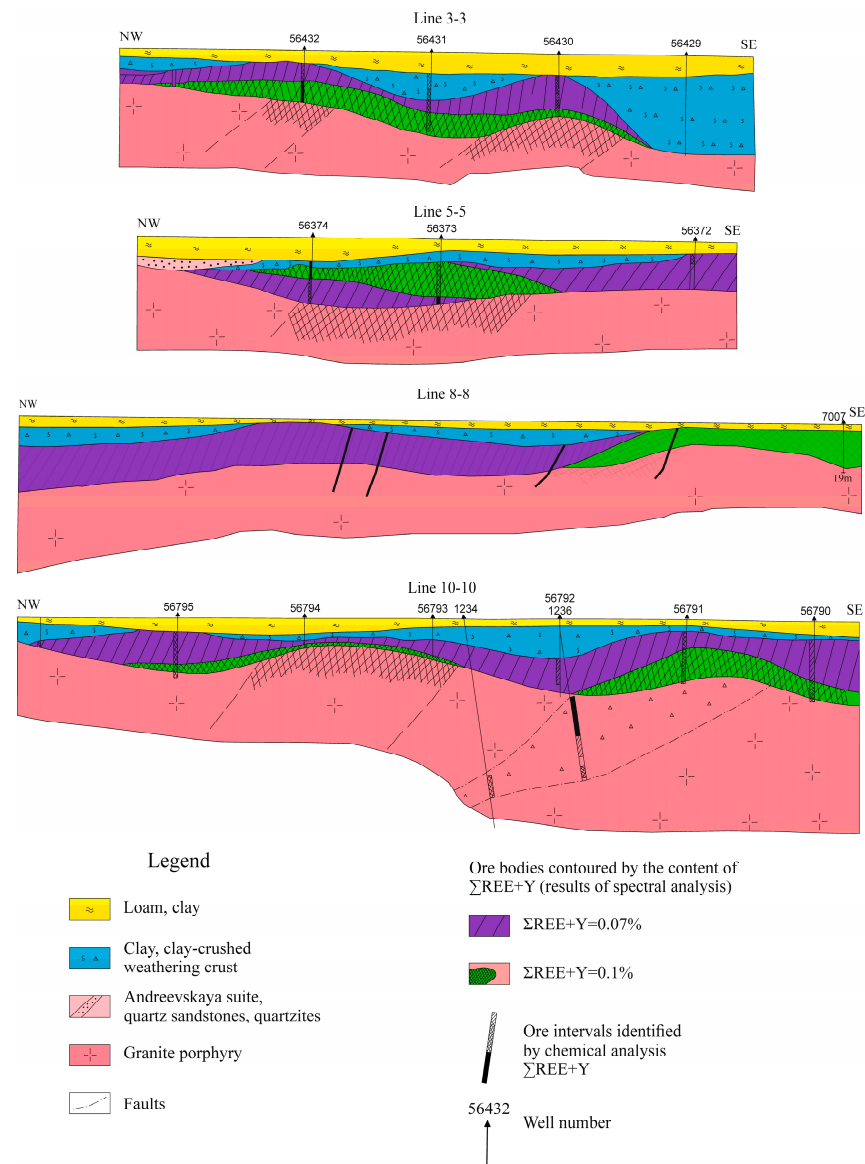


Figure 3. Geology of the Syrymbet ore field, simplified from Raport (2019) [23]. Lines 3–3, 5–5, 8–8, and 10–10 show profiles selected for investigation and exploration (constructed alongside lines showed in Figure 2), with the ore bodies contoured by the sum of REE and yttrium quantities.

A field digital database from eight drill wells was used to construct the geological profiles. The ore body's boundaries, with ΣREE cut-off grades of 0.07% and 0.1%, were adopted as the basis for the wireframe model, and these ranges were selected according to deposit categories A and B (so-called recognised and developed deposits) in accordance with the laws in Kazakhstan.

The spatial boundaries of the ore deposits were modelled using Micromine computer software, and the work was carried out in several stages, depending on the modelled object.

The stages were as follows: the development of a database (DB) structure to store basic information about the geological survey data; the entering and analysis of preliminary information into the geological database; the interpretation of geological exploration data; and the creation of wireframe models of spatial volumes. In detail, the methodology of modelling included the following: 1. A DB structure was developed for storing primary information about the geological survey data. 2. A mechanism for averaging the intervals of primary geological sampling was present, which is one of the main features of the creation and maintenance of a database of exploration wells for mineral deposits. The database included tools for structural filtering using a set of indicators, triggers, calculated fields (mathematical, statistical, and logical functions), statistical analyses, and charts. Using the mathematical statistics apparatus, the correctness of the entered primary data, the presence of mixed-content populations, and the cut-off content for the useful components in the ore were determined. 3. The next stage of modelling involved the analysis and interpretation of geological data in the wells and the determination of mineralisation zones according to the cut-off values. As a result of the interpretation, closed contours describing the mineral varieties and rocks were created. Similarly, ore bodies were contoured for all geological profiles. After entering the data, it was loaded into a three-dimensional space to check the correctness of the structure. 4. In the next stage of modelling, three-dimensional wireframe models were created detailing the morphology of ore bodies. They were built not only for ore bodies, but also for mineral varieties in the contours of ore bodies and varieties of overburden rocks. 5. At the final stage of modelling, three-dimensional block models were created with a visualisation of the distribution of the ore element contents over the ore deposit. This created empty block models bounded by wireframes; the interpolation of the component content values was based on the established distribution law and refinement of rock contours according to specific conditions. 6. The generated three-dimensional model of the deposit can be used to calculate the deposit reserves or its sections, perform geological and economic assessments, plan tasks, and determine the economically viable mining contours. The main difference in the models created using the Micromine computer program is the possibility of their further use and refinement based on the results of the deposit development. In this case, the total size of the model is limited only by the hardware capabilities of the computer.

A linear distribution of mineralisation was assumed, due to the origin of the deposits and the core development in the weathering processes, which has been documented in IAD-REE-type deposits.

3. Results

3.1. Rare Earth Elements in the Weathered Crust

The spectral analysis results showed the presence of rare earth elements, both within and outside the deposit area, with a significant predominance of light lanthanides (LREEs) of the cerium series (La, Ce, Pr, Nd, Sm, and Eu). There were smaller quantities of heavy lanthanides (HREEs) of the yttrium series (Y, Gd, Tb, Dy, Ho, Er, Tm, Yb, and Lu). In the Shok-Karagay field, the average volume of the cerium series was 3.738 g/t, and that of the yttrium series was 954 g/t. Therefore, the average Pr content varied from 0 to 7000 g/t, averaging 1718 g/t, and the Nd was from 1000 to 3000 g/t, averaging 1508 ppm (Table 1). The average concentrations of other rare earth elements across the wells varied as follows (g/t): La, 43–200, average of 134; Ce, 57–206, average of 116; Sm, 100–300, average of 225; Eu, 22–100, average of 37; the yttrium series: Y, 31–106, average of 69; Gd, 100–200, average of 125; Tb, 100–200, average of 159; Dy, 0–300, average of 254; Ho, 0–20, average of 17; Er, 0–364, average of 274; Tm, 0.28–0.85, average of 0.58; Yb, 2.2–39, average of 17; Lu, 0–200, average of 38. In both the bedrock and the weathering crust, light lanthanides significantly prevailed over heavy ones. Rare earth minerals (monazite, rhabdophane, and parisite) were also dominated by light lanthanides and commonly contained radioactive thorium and uranium.

Table 1. Content of REEs in the Shok-Karagay site’s weathering crust according to the results of chemical analysis (ASA, in ppm).

Σ REE	Elements of Cerium Series (LREEs)							Elements of Yttrium Series (HREEs)							
	La	Ce	Pr	Nd	Sm	Eu	Y	Gd	Tb	Dy	Ho	Er	Tm	Yb	Lu
3940	250	200	1000	1000	300	30	200	100	200	300	20	300	2.5	25	10
49.8	10	15	5	5	1.5	0.2	5	1	1	2	ND	2	0.5	1.5	0.1
3740	200	200	1000	1000	300	30	70	100	200	300	20	300	0.7	7	10
281	50	70	7	50	6	1	60	7	6	10	ND	6	0.5	6	1
3450	50	20	1000	1000	300	30	100	100	200	300	20	300	1	15	10
134	20	10	2	20	3	0.5	50	10	1	7	ND	4	0.5	5	1
3460	70	70	1000	1000	300	30	50	100	200	300	20	300	0.5	5	10
167	30	20	7	40	5	1	40	10	4	4	ND	4	0.4	5	1
3640	142	123	1000	1000	300	30	105	100	200	300	20	300	1.2	13	10
158	28	29	5	29	3.9	0.68	39	7	3	0.8	ND	4	0.48	4.4	0.8

Note: Generally, for the wells of the Shok-Karagay site, Σ REE of the cerium series—2595; Σ REE of the yttrium series—1049 (sp. an.). (sp. an.)—spectral analysis; ND—not detected.

3.2. Rare Earth Accessory Minerals

3.2.1. Mineral Composition of Primary Ores in the Deposit’s Bedrock Subsection

The mineralogical analysis confirmed that the main rare minerals were tantalum–columbite, cassiterite, and wolframite. The secondary one was ilmenorutile. The dominant rare earth mineral was monazite, and the secondary one was parisite. The radioactive minerals included thorite and orangite. The rare and accessory minerals included ilmenite, magnetite, titanomagnetite, zircon, hematite, pyrite, chalcopyrite, arsenopyrite, rutile, galena, and chromspinel. The major gangue minerals were common quartz, chlorite, mica, and, rarely, potassium feldspar, whereas the secondary minerals included tourmaline, garnet, amphibole, epidote–zoisite, and different mica varieties. Moreover, titanite, apatite, fluorite, spinel, kyanite, and sillimanite were indicated. Manganese oxides were determined to be components of hypergenic minerals (Table 2).

The bedrock primarily consisted of ilmenorutile, rutile, hematite, magnetite, ilmenite, titanomagnetite, and zircon, and all these minerals commonly or sometimes contain REEs (Figure 4). In addition to niobium in subordinate amounts, ilmenorutile, in close intergrowth with rutile in silicified and sericitised granite porphyries, contained tantalum and tungsten. REEs may be present in ilmenorutile as an isomorphic impurity (Figure 4). Rutile, present as irregular, sparse phenocrysts in granite porphyries of sericitised and explosive breccias, contained niobium amounts between 3 and 3.5 wt.%. The Fe and Ti-Fe minerals, hematite, magnetite, ilmenite, and titanomagnetite, are accessory minerals that form rare irregular small phenocrysts in the rock mass of the host’s rare earth mineralisation. The ilmenite grain analysis showed niobium impurities (0.35%). As an accessory mineral, zircon was present as rare phenocrysts in granite porphyries and contained 0.48–0.93 wt.% of hafnium. Rutile and ilmenorutile were closely associated with zircon, and their accumulation sites may contain rare earths. In host rocks with rare earth mineralisation, the following REE minerals were found: monazite, rhabdophane, yttrium parisite, and, in the minority, thorite and its mineralogical variety, orangite. Monazite, (REE)PO₄, was found in granite porphyry parent rocks, which developed rare phenocrysts of magnetite, titanomagnetite, ilmenite, and zircon. REE phases formed small-range crusts on the grains of the zircon and monazite, and the size of the crusts was up to 10 × 50 μm². The rare earth elements in monazite accounted for 54.15 wt.% (La, Ce, Pr, Nd, Sm, Eu, Gd, and Dy), out of which the yttrium subgroup elements (Gd and Dy) amounted to 2.97 wt.% (Table 3). Monazite and ilmenite often contained various additives, including Th and U (Figure 4).

Silicorhabdophane (REE, Ce)PO₄·H₂O is a variety of rhabdophane, a phosphate of the cerium rare earth subgroup. This mineral occurs as a part of brecciated rock containing quartz and potassium feldspar fragments in a siliceous mass. The rock contains irregular phenocrysts of rutile and isolated rare phenocrysts of ilmenite. The mineral grains are very small, and do not exceed 3 × 5 μm². Elements of the cerium series (La, Ce, Pr, and Nd) and radioactive Th were found in silicorhabdophane (Table 3).

Table 2. Mineral composition of the primary rocks of the Shok-Karagay deposit based on microscopic analysis.

Rare-metal-bearing Minerals	
Tantalite–Columbite	+++
Cassiterite–Wolframite	+++
Ilmenorutile	++
Rare-earth-element-bearing Minerals	
Monazite	+++
Parisite	++
Rhabdophane	++
Thorite	+
Orangite	+
Gangue Minerals	
Quartz	+++
Chlorite	+++
Micas	+++
K-feldspar	+++
Tourmaline	++
Garnet	++
Amphibole	++
Epidote–zoisite	++
Sphene	+
Apatite	+
Fluorite	+
Spinel	+
Cyanite	+
Sillimanite	+
Ilmenite	+
Magnetite	+
Titanomagnetite	+
Zircon	+
Hematite	+
Pyrite	+
Chalcopyrite	+
Arsenopyrite	+
Rutile	+
Galena	+

Explanations: +++ major mineral phases, ++ secondarily important mineral phases, + minor mineral phases.

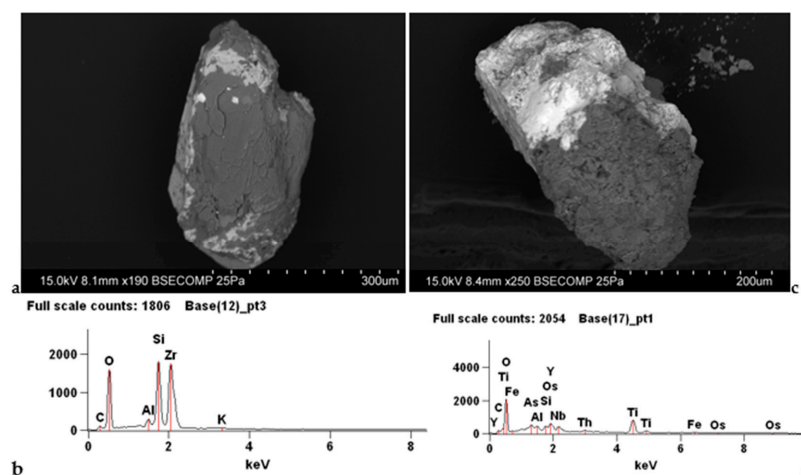


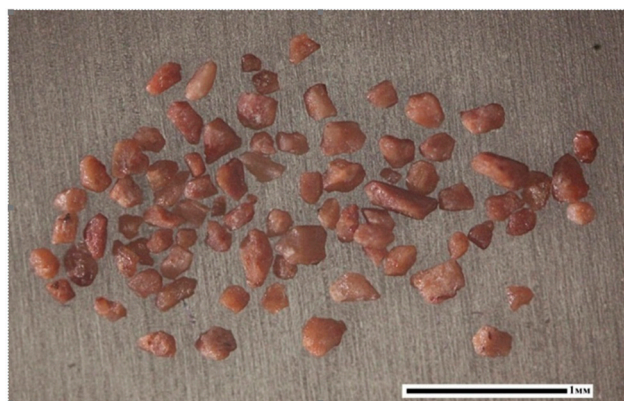
Figure 4. SEM analysis of zircon and Fe–Ti–Nb–REE mineral associations. Ilmenite with REEs and rare metal additives: (a) BSE image of zircon (white) intergrowths with feldspar grain (dark grey) and (b) EDS spectrum of zircon (ZrSiO₄ by stoichiometry; Al and K were measured from the background). (c) Fe–Ti–Nb–REE mineral, and (d) EDS spectrum of ilmenorutile with REEs and rare metal additives.

Table 3. Chemical compositions of major REE phases: monazite, silicorhabdophane, and parisite (ND—not detected).

	Major Compounds (in wt.%)			
	Monazite	Silicorhabdophane		Parisite
F	1.56	ND	ND	7.47
Al ₂ O ₃	ND	ND	ND	0.96
SiO ₂	ND	11.4	11.7	2.84
P ₂ O ₅	28.8	30	31.8	ND
CaO	3.28	2.48	2.78	2.39
TiO ₂	ND	ND	ND	0.53
Fe ₂ O ₃	ND	0.84	ND	4.78
Y ₂ O ₃	ND	ND	ND	7.04
Rare earth elements (in wt.%)				
La ₂ O ₃	10.7	13.6	13.7	13.9
Ce ₂ O ₃	27.6	29.7	29.1	18.4
Pr ₂ O ₃	2.22	2.09	ND	2.44
Nd ₂ O ₃	8.86	7.58	8.2	10.8
Sm ₂ O ₃	1.56	ND	ND	2.73
Eu ₂ O ₃	0.34	ND	ND	0.76
Gd ₂ O ₃	2.14	ND	ND	2.63
Tb ₂ O ₃	ND	ND	ND	1.07
Dy ₂ O ₃	0.83	ND	ND	1.88
ThO ₂	0.7	3.97	6.92	1.9
UO ₃	1.64	ND	ND	ND
SUM	90.23	101.66	104.2	82.52

Parisite CaCe₂(CO₃)₃F₂ was found in sericitised porphyry granite. The ore minerals in this rock included hematite, ilmenite, and rutile and accounted for 3–5% of the rock mass. Fluorine—an element of the parisite structure—was also present in porphyry granite as fluorite (5–8% of rock mass). Parisite occurred in clusters of small grains of 1–10 μm. Parisite contained elements of LREEs, HREEs, and radioactive thorium. These rare earth elements constituted 61.65% of the mineral mass (and consisted of Y, La, Ce, Pr, Nd, Sm, Eu, Gd, Tb, and Dy). The content of Y₂O₃ (7.04%) and ThO₂ (1.9%) can be attributed to yttrium parisite (Table 3).

Thorite and orangite ThSiO₄ were related to minor minerals in the bedrock analysis. These minerals were commonly located outside of the Shok-Karagay ore area and were often found sporadically. A variety of thorite–orangite was also present in some samples (Figure 5).

**Figure 5.** Orangite grains (thorite variety) separated from the heavy fraction (binocular microscope, opaque light). Scale bar: 1 mm.

3.2.2. Mineral Composition of the Shok-Karagay Ores of the Weathering Crust

Weathering crusts consist mostly of clay minerals, and among them predominates kaolinite. Analysis of heavy fractions from the weathering crusts, obtained from drill holes in the Shok-Karagay deposit, indicated cassiterite and wolframite as the main minerals and ilmenorutile as the secondary mineral. Monazite was the primary rare earth mineral and parisite was a minor mineral. The rare and accessory minerals included magnetite, titanomagnetite, hematite, zircon, rutile, anatase, and pyrite. The common gangue minerals (light fraction) included quartz, albite, and sericite. The minor ones were tourmaline, amphiboles, pyroxenes, chlorites, and the epidote–zoisite group. The supergene minerals included leucoxene, goethite, hydrogoethite, manganese oxides, ferruginous ochres, and clays (kaolinite).

3.2.3. Isomorphic REE Additives in Gangue and Accessory Minerals

Gangue minerals, including the rock-forming and accessory minerals of the weathering crust, e.g., kaolinite, wolframite, ilmenorutile, zoisite, zircon, titanite, fluorite, and mica, may contain isomorphic impurities of rare earth elements (Figures 4 and 6). The crystals of differently coloured zircons (yellow or orange) containing fine inclusions, including mica and orthite (allanite group), showed the presence of rare earth elements: Y (70–75 g/t), La (20–500 g/t), radioactive Th (up to 30 g/t), U (50–350 g/t), and the rare metal Nb (30–10 kg/t).

Monazite is the primary carrier of rare earth elements from the cerium group. The minor mineral fluorocarbonate–parisite also contains rich quantities of cerium group elements, yttrium (7–8%), and other rare earth elements of the yttrium group in smaller amounts. Secondary radioactive minerals (such as thorite and its variety, orangite), other major and minor Ta-Nb-Ti-W minerals (tantalum–columbite, wolframite, and ilmenorutile), rock-forming minerals (hydromicas and feldspars), and accessory minerals (ilmenite, titanite, zircon, zoisite, fluorite, and apatite) may contain REE additives.

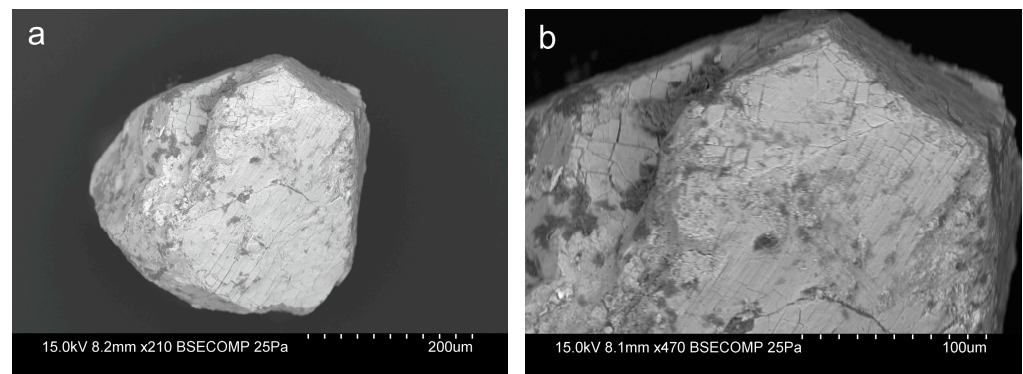


Figure 6. (a) BSE image of zircon grain (white) and (b) enlargement of the upper part of the image (a) with mica-like intergrowths (grey).

3.3. Wireframe Model of the Shok-Karagay Deposit's Lithological Structure

All wireframe models of the Shok-Karagay field's lithological structure were outlined along the lithological boundaries obtained from the geological well column data and geological sections drawn along lines 3–3 and 5–5 (South Shok-Karagay) and 8–8 and 10–10 (North Shok-Karagay) (Figures 3 and 7). Three primary ore-bearing zones were designated: two zones with a northeastern orientation (Northeastern I and II) and one zone with a northwestern orientation (Northwestern, Figure 2). Northeastern zone I was the most intensively studied of these ore zones. We modelled these zones for ore bodies with grades between 0.10% and 0.07% of the REE sum. The zone was traced using appraisal drilling in sections every 200–400 m, to a depth of 300–350 m at a distance of 1800 m. The maximum content of rare earth elements in wells Nos. 7002 and 7008, exposed along the

northeastern ore zone, reached 0.06 wt.% and up to 0.1 wt.% in well No. 7003. Below the REE-rich bedrocks, granite porphyry intrusion was found. The weathering crust lay almost horizontally and mirrored the upper surface of the felsic intrusion.

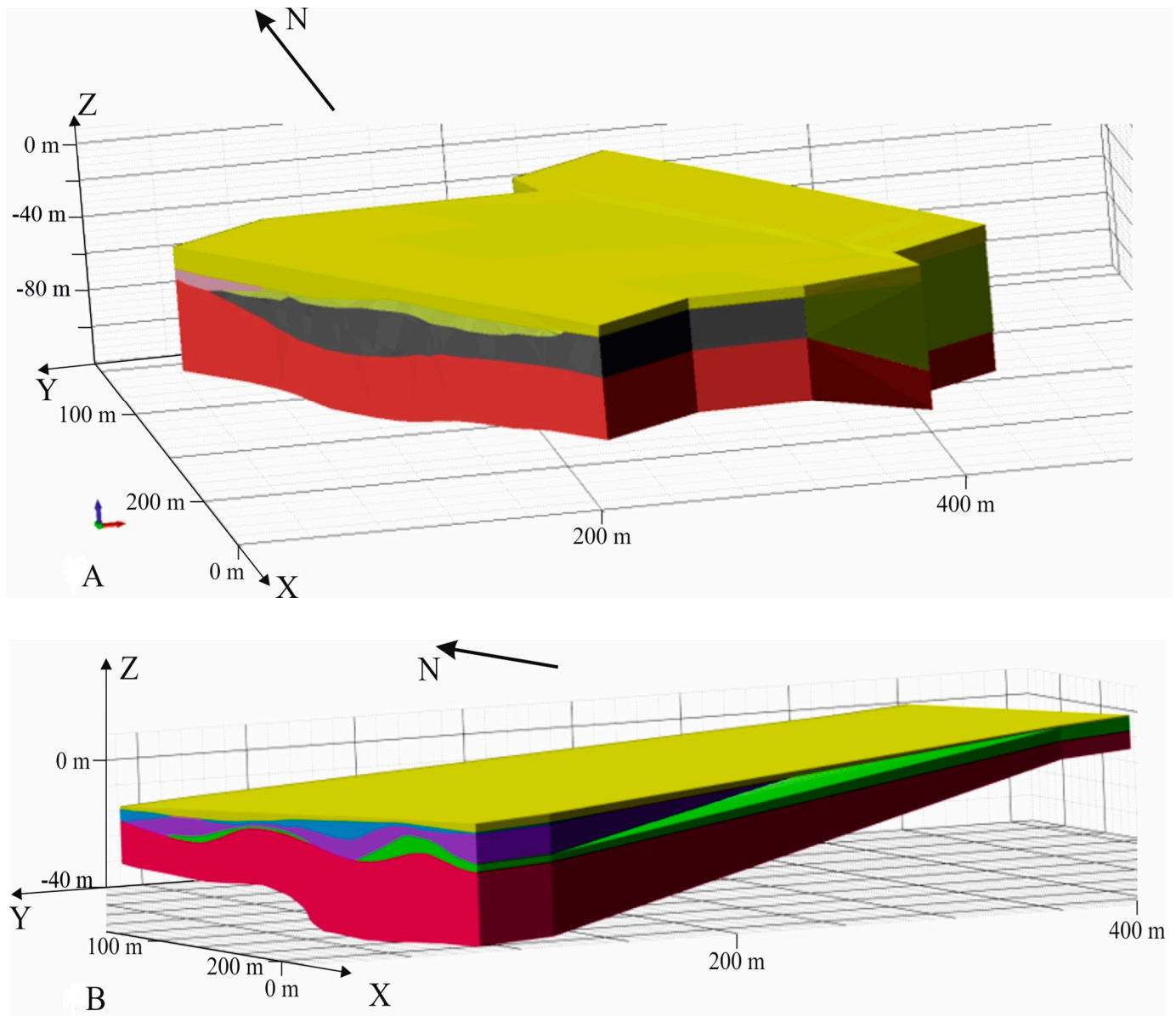


Figure 7. Three-dimensional lithological model of the structure of the deposit. (A) Shok-Karagay South: yellow—blanket deposits; green and dark grey—ore-bearing weathering crust; pink—quartz sandstones and quartzites; red—intrusion. (B) Shok-Karagay North: yellow—blanket deposits; blue—clay and clay-crushed weathering crust; green and purple—ore-bearing weathering crust; red—intrusion.

3D wireframe model analysis of the southern Shok-Karagay deposit helped determine the shapes and sizes of the deposit bodies. The ore body shapes were uncomplicated, with relatively simple structures in the form of an elongated bed. The geometric parameters of the site were 1000×350 m (Figures 8 and 9). These simple ore body shapes were predetermined by the development of a linear weathering crust. Moreover, ore bodies with different REE contents had different thicknesses, and the thickest ore body constituted a layer with REE content not exceeding 0.07%. The visualisation of REE concentrations in

the deposit showed that rare earth elements were the most widespread in the range up to 0.07%, with an increase to 0.1% in its southern part.

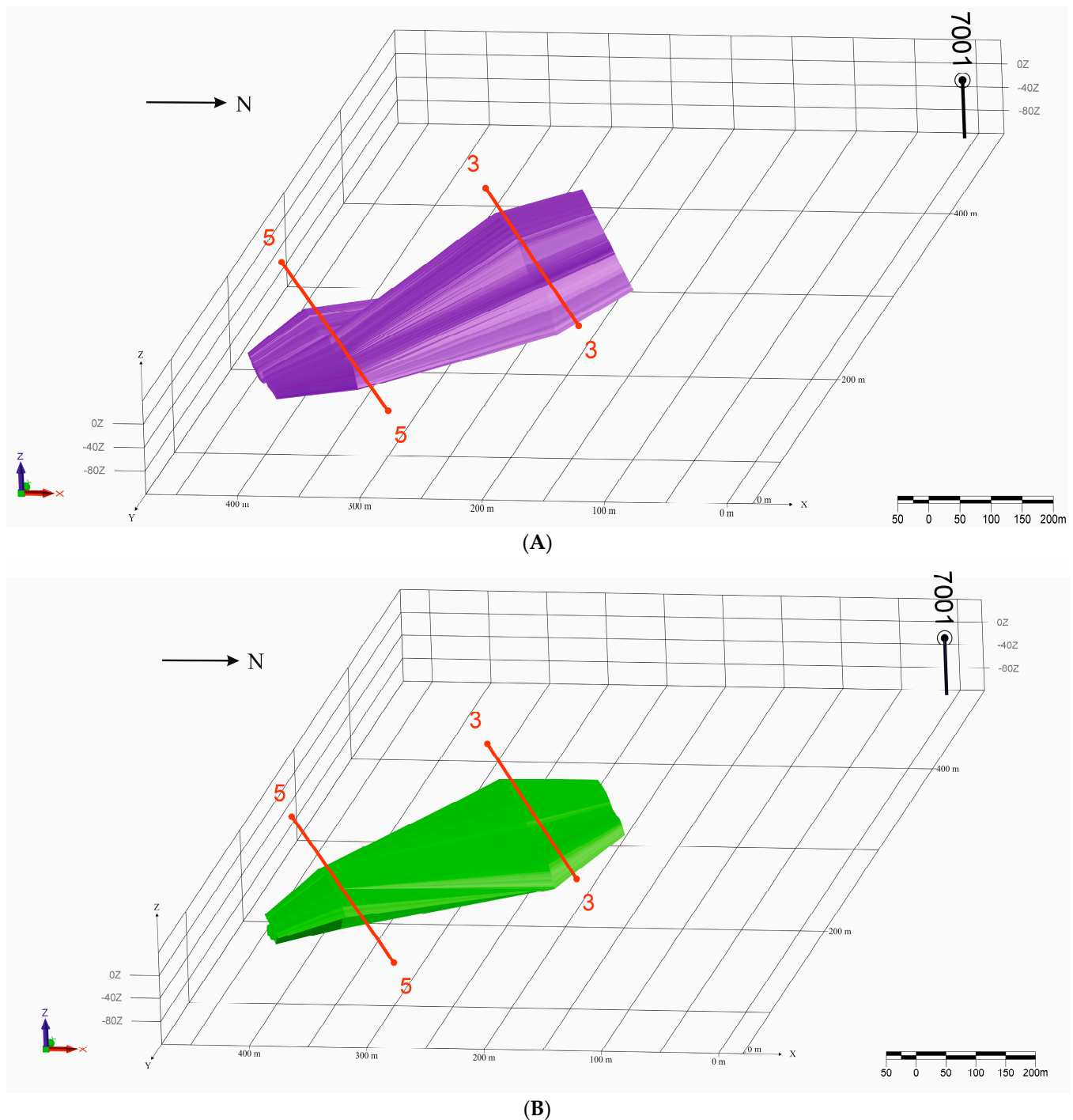


Figure 8. (A,B) Three-dimensional wireframe models of ore bodies in the southern section of Shok-Karagay with different REE grades ((A)—0.07 wt.%, (B)—0.10 wt.%) running through exploration profiles 3–3 and 5–5. The contours of the ore bodies indicated high regularities and a homogenous structure, with thicknesses reaching 40 m and lengths reaching 350 m.

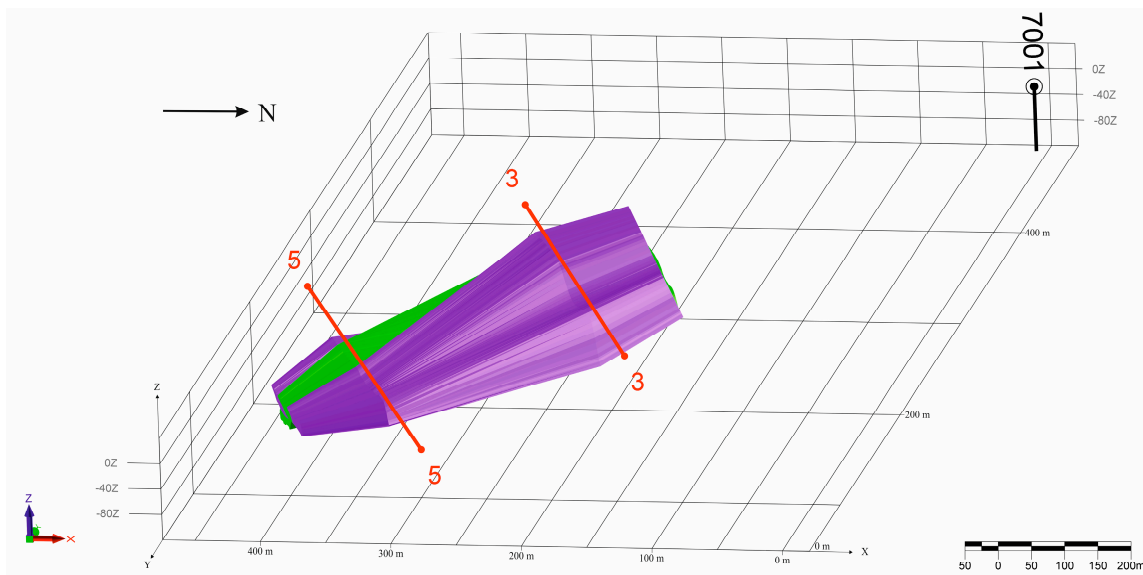


Figure 9. Three-dimensional model of an ore body in the southern Shok-Karagay deposit with different REE contents, modelled with 0.10 wt.% REEs—green, 0.07 wt.% REEs—purple.

The ore body models in the northern Shok-Karagay deposit were constructed as geological sections (Figure 3: sections 8–8 and 10–10) and delineated by the cut-off of a sum of rare earth elements contents of 0.10 and 0.07 wt.%. 3D model analysis indicated that the ore body shapes were simple and in the form of an elongated bed in Shok-Karagay’s northern section with wedges in the SW–NE direction. According to computer simulation calculations, the dimensions of the section were $1047 \times 385 \text{ m}^2$ (Figures 10 and 11).

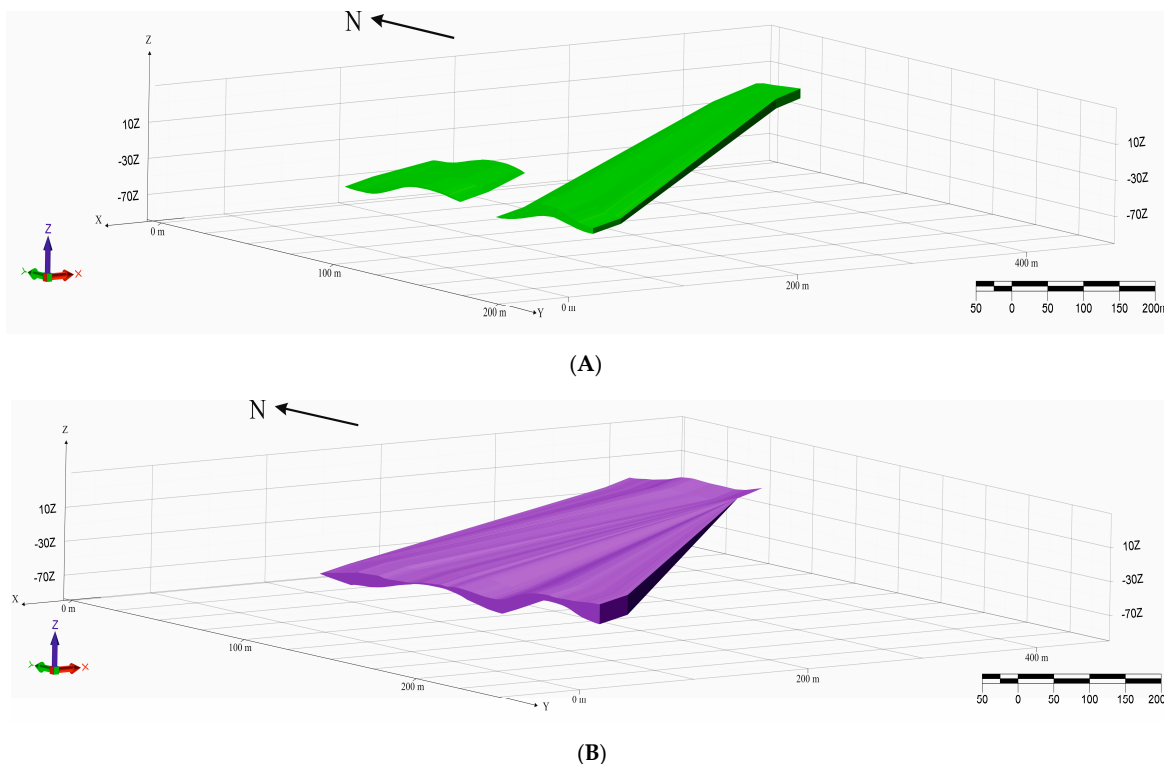


Figure 10. Three-dimensional wireframe model of ore bodies with different REE contents: (A) green—0.1 wt.%; (B) purple—0.07 wt.%.

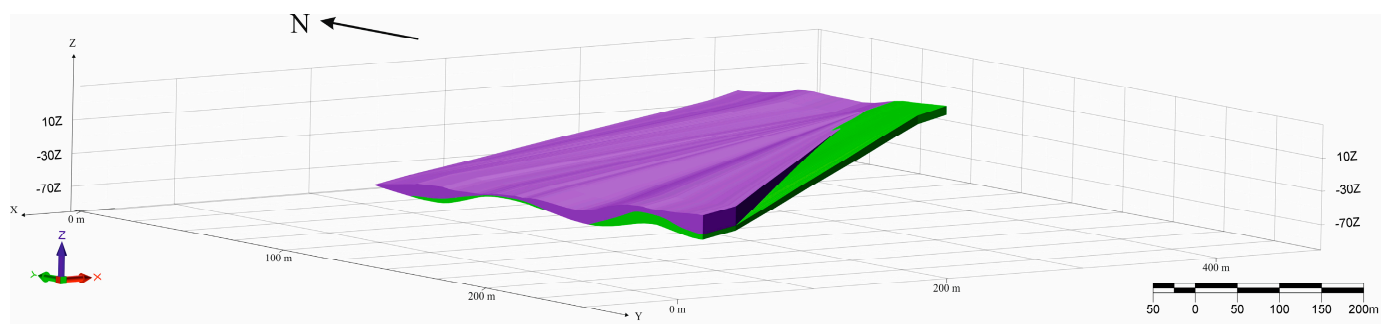


Figure 11. Three-dimensional wireframe model of an ore body from the northern section of Shok-Karagay: green—0.07 wt.% and purple—0.1 wt.% of REEs.

4. Discussion

Based on drilling data, the Shok-Karagay North and Shok-Karagay South ore deposits were examined, and showed similar parameters. They were relatively simple due to their shape and size, and the northern and southern parts of the deposits indicated a similar architecture of the ore bodies.

Three main ore-bearing zones were designated in the Shok-Karagay North area: two zones with a northeastern orientation (Northeastern I and II) and one zone with a northwestern orientation (Northwestern, Figure 2). Northeastern zone I was modelled for ore deposits ranging from 0.1 to 0.07 wt.% of the REE totals. The zone was marked by exploratory drilling in sections every 200–400 m to a depth of 300–350 m at a distance of 1800 m. The maximum content of rare earth elements in drill holes Nos. 7002 and 7008 along the northeastern ore zone reached 0.06 wt.%, and in drill hole No. 7003, it reached up to 0.1 wt.%.

The distribution of REEs strongly depended on the hydrothermal and pneumatolytic–hydrothermal processes of alteration, which caused concentrations of rare earth elements within albitised and greisenised granites and granite porphyries of the Dalnen system [18–20]. After hydrothermal and post-magmatic alterations, paleoweathering processes took place, forming a crust on the surface of the igneous rocks and causing alterations to its primary components with the possible differentiation of the REE group (into LREEs—cerium series and HREEs—yttrium series). Therefore, the closer the source, the higher the content of rare earth elements in the weathering crusts in Shok-Karagay North (Figures 3 and 7) and South (Figures 3 and 8), as indicated by the models (Figures 7–12).

The Shok-Karagay deposits were dominated by Fe–Ti–Nb mineral associations represented by the following minerals: ilmenorutile, rutile, hematite, magnetite, ilmenite, titanomagnetite, and, commonly, zircon. The main ore minerals were tantalum–columbite, cassiterite, and wolframite, and other rare earth components included the commonly occurring monazite, yttrium parisite, and orthite in smaller quantities. This mineral association consistently agrees with the mineralogical differentiation of other ion-adsorption deposits formed in weathering crusts in the Syrymbet field and northern Kazakhstan (the Kundybai deposit) [19–21]. In addition to REEs adsorbed in ionic form on clay minerals, the accessory minerals in this deposit type are an important source of rare metals because they are easily separated from a heavy fraction from the weathered cover. The total amount of rare earth elements in weathered crust (Table 3) depends on the weathering effect of the primary granitic rocks [20]. The concentration and REE type are mainly related to two factors: the source rocks of the sediments and the concentration of REE-containing minerals in the terrigenous sediments [24]. In Bayan Obo, the most important REE deposit in Southern China, the sum of the LREE group mostly prevailed over that of the HREE group [25] and reached 60% [26], whereas in Shok-Karagay, the sum of LREEs reached 67% and was 2595 ppm. In Shok-Karagay, as in the Bayan Obo deposits, the geochemical association of the accessory minerals belonged to Fe–Ti–Nb phases, mainly in the form of a heavy fraction [24,26,27]. This may be due to fractionation of REEs during the weathering processes

and a possible increase in the LREE content in the fine fraction [28,29]. It is worth noting that the concentration level of rare earth elements in the ores of the Shok-Karagay deposit are comparable to that of the large deposits in Kazakhstan, such as Kundybai, which also formed through weathering processes. A similar REE content was determined in Kundybai deposits, which averaged 600–2000 ppm of REEs, with an increase in the thickness of the beds by 40–60 m [23,30]. The total REO content in Shok-Karagay increased in the central part of the beds and slowly decreased in the outer part of the deposits, which was consistent with the development of the weathering.

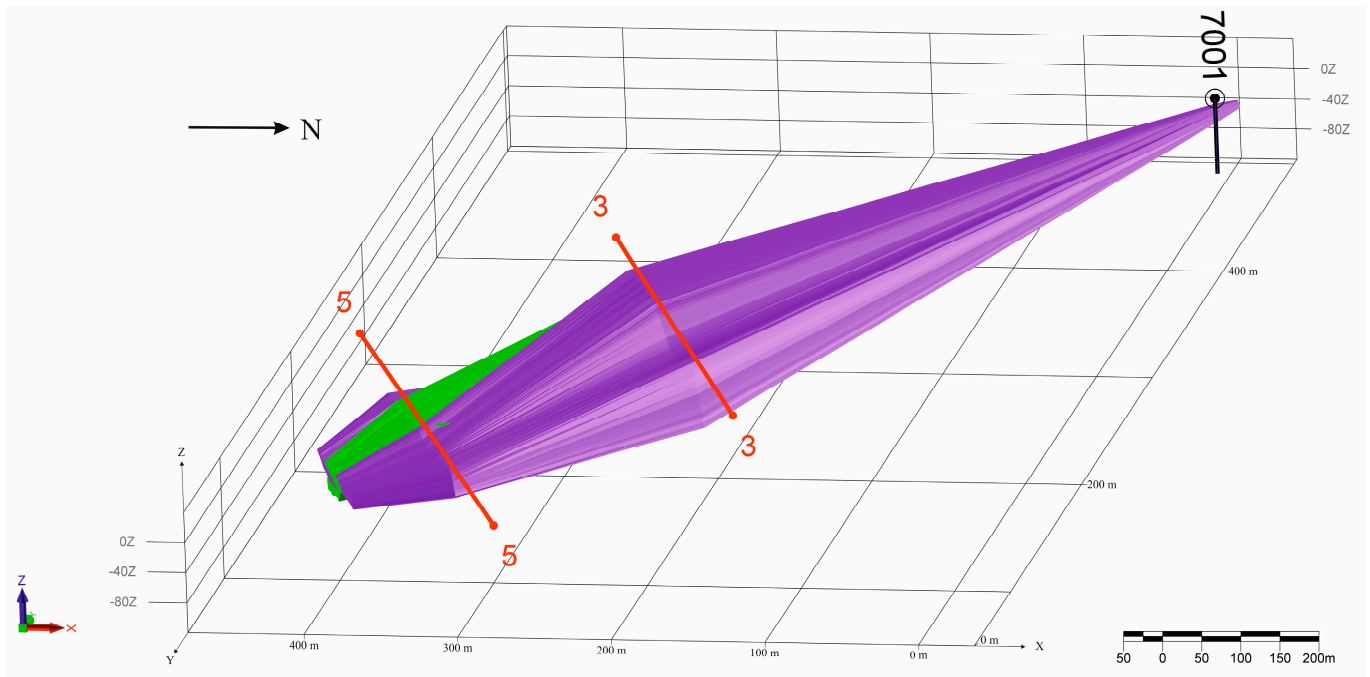


Figure 12. Three-dimensional model of an ore body viewed with prospective areas of different REE contents: green—0.1% of total REEs and purple—0.07% of total REEs. The structures of the bed of deposits were modelled along the 5–5 and 3–3 cross-sections with cut-offs of 0.07% and 0.10 wt.% REEs; a wedge shape of the bed was indicated, oriented towards the SW–NE direction with a thickness ranging from 40 to 1800 m.

Visualisation of the REE content showed that the most common REE content was below 0.07%, which increased to 0.1% in the northeastern part. Ore bodies with different REE contents developed differently within the deposit: an ore body with a 0.07% REE content was observed to be continuous, whereas an ore body outlined by a 0.1% REE content formed two separate flat bodies (Figures 7–12). Both Shok-Karagay sites had simple structures occurring in the form of elongated beds. Moreover, the distribution of rare earth elements was zonal; the content of rare earth elements in the upper horizons was below 0.07%, whereas in the lower horizons, the content of rare earth elements reached 0.10%.

The spectral analysis obtained from the drillings showed the presence of rare earth elements with contents below the cut-off grade (0.07%), suggesting a greater extent of the ore zones. The 3D morphology of the extended ore deposit was visualised by moving the deposit boundary in the Shok-Karagay South site’s wireframe model up to well No. 7001. In this case, the ore bodies extended another 2 km (Figure 7). The entire spectrum of lanthanides, ytterbium, lanthanum, cerium, gadolinium, and yttrium determined in selected samples using a semiquantitative spectral analysis was similar in both parts of the deposit.

A distinctive feature of the Shok-Karagay deposit is its complex rare metal and rare earth metallogenetic specialisation, determined by its location in a single node with the large Syrymbet tin deposit [22]. The entire ore cluster is unevenly covered by different mineralisation phases (albitization, quartz–beryllium, and hydrothermal quartz–fluorite mineralisa-

tion [20]), determining the complex rare earth compositions of the Shok-Karagay deposit's weathering crust and the deposit's architecture. Recent discoveries of REE deposits in Madagascar provide new prospecting areas of regolith-hosted clay deposits [8,23,27]; however, this deposit and the other new deposits in Central and Eastern Asia should also be considered global resources.

5. Conclusions

The REE ore minerals in the Shok-Karagay deposits occur in a weathering crust form represented by the following associations: ilmenorutile, rutile, hematite, magnetite, ilmenite, titanomagnetite, and zircon.

In the weathering crust of the Shok-Karagay field, the sum of the elements from the cerium series prevailed over that of the yttrium series by four times on average, according to semiquantitative spectral analysis. The rare earth minerals occurring were monazite as the primary mineral and parisite as the secondary one. REEs, in the form of isomorphic impurities, were contained in primary ore minerals: namely, cassiterite and wolframite, ilmenorutile in minor minerals, and other rock-forming and accessory minerals (kaolinite, mica, zoisite, titanite, zircon, and fluorite). According to electron probe microanalysis, rare earth mineralisation in the host bedrock is represented by phosphates, namely monazite, silicorabdophane, and fluorocarbonate parisite, with the addition of radioactive elements, namely Th and U.

The Shok-Karagay North and South ore deposits identified by well testing showed a relatively simple structure, elongated to the northwest due to the fault directions and comprising nearly horizontal ore bodies of thicknesses not exceeding 40 m in both fields. The study of materials from the Shok-Karagay North ore body and 3D models showed that the main ore body is outlined between these exploration wells, where the cumulative content of rare earth elements varies from 0.1% to 0.07%. The prospects of the Shok-Karagay deposit can be defined by extending the ore bodies' boundaries along the faults.

Author Contributions: Conceptualisation, K.T., L.I. and A.D.-C.; methodology, K.T., L.I. and A.D.-C.; software, M.S.; validation, D.M. and M.K.; formal analysis, K.T.; investigation, D.M., M.K. and A.D.-C.; data curation, M.K.; resources, K.T. and L.I.; writing—original draft preparation, L.I. and A.D.-C.; writing—review and editing, M.S. and A.D.-C.; visualisation, D.M.; supervision, K.T.; project administration, K.T. and L.I.; funding acquisition, K.T. All authors have read and agreed to the published version of the manuscript.

Funding: This research was funded by the Ministry of Ecology, Geology, and Natural Resources of the Republic of Kazakhstan, grant number BR10264324. The SEM-EDS investigations were funded by the Geography and Geological Department of the Adam Mickiewicz University in Poznań, Poland.

Data Availability Statement: The data presented in this study are available on request from the corresponding author. The data are not publicly available due to company secrets and licensing restrictions.

Acknowledgments: The authors thank Danuta Michalska for conducting the SEM-EDS analysis.

Conflicts of Interest: The authors declare no conflict of interest.

References

1. Goodenough, K.M.; Wall, F.; Merriman, D. The Rare Earth Elements: Demand, global resources, and challenges for resourcing future generations. *Nat. Resour. Res.* **2018**, *27*, 201–216. [CrossRef]
2. Wall, F. Rare Earth Elements. In *Encyclopedia of Geology*, 2nd ed.; Alderton, D., Elias, S.A., Eds.; Academic Press: London, UK, 2021; pp. 680–693.
3. Wall, F. Rare earth elements. In *Critical Metals Handbook*, 2nd ed.; Gunn, G., Ed.; John Wiley & Sons: Chichester, UK, 2014; Volume 3, pp. 312–339. [CrossRef]
4. Li, Y.H.M.; Zhao, W.W.; Zhou, M.-F. Nature of parent rocks, mineralization styles and ore genesis of regolith-hosted REE deposits in South China: An integrated genetic model. *J. Asian Earth Sci.* **2017**, *148*, 65–95. [CrossRef]
5. Statista. Available online: <https://www.statista.com/statistics/277268/rare-earth-reserves-by-country/> (accessed on 13 September 2023).

6. Voncken, J.H.L. *The Rare Earth Elements: An Introduction (Springer Briefs in Earth Sciences)*, 1st ed.; Springer: Cham, Switzerland, 2016. [CrossRef]
7. Hellman, P.; Duncan, R. Evaluating Rare Earth Element Deposits. *ASEG Ext. Abstr.* **2018**, *1*, 1–13. [CrossRef]
8. Borst, A.M.; Smith, M.P.; Finch, A.A.; Estrade, G.; Villanova-de-Benavent, C.; Nason, P.; Marquis, E.; Horsburgh, N.J.; Goodenough, K.M.; Xu, C.; et al. Adsorption of rare earth elements in regolith hosted clay deposits. *Nat. Commun.* **2020**, *11*, 4386. [CrossRef]
9. Omirserikov, M.S.; Duczmal-Czernikiewicz, A.; Isaeva, L.D.; Asubaeva, S.K.; Togizov, K.S. Resource prediction for rare metal deposits based on the analysis of ore-controlling factors (in Russia). *Izv. RK NAS Geol. Tech. Sci. Ser.* **2017**, *3*, 35–43.
10. Broom-Fendley, S.; Heaton, T.; Wall, F.; Gun, G. Tracing the fluid source of heavy REE mineralization in carbonatites using a novel method oxygen isotope analysis in apatite: The example of Songwe Hill Malawi. *Chem. Geol.* **2016**, *440*, 275–287. [CrossRef]
11. De Kemp, E.A.; Monecke, T.; Sheshpari, M.; Girard, E.; Lauzière, K.; Grunsky, E.C.; Schetselaar, E.M.; Goutier, J.E.; Perron, G.; Bellefleur, G. 3D GIS as a support for mineral discovery. *Geochem. Explor. Environ. Anal.* **2011**, *11*, 117–128. [CrossRef]
12. Schetselaar, E.; Pehrsson, S.; Devine, C.; Lafrance, B.; White, D.; Malinowski, M. 3-D Geologic Modeling in the FlinFlon Mining District, Trans-Hudson Orogen, Canada: Evidence for Polyphase Imbrication of the Flin Flon-777-Callinan Volcanogenic Massive Sulfide Ore System. *Econ. Geol.* **2016**, *111*, 877–901. [CrossRef]
13. Joly, A. Mineral systems approach applied to GIS-based 2D-prospectivity modelling of geological regions: Insights from Western Australia. *Ore Geol. Rev.* **2015**, *71*, 673–702. [CrossRef]
14. Mars, J.C. Mineral and Lithologic Mapping Capability of WorldView 3 Data at Mountain Pass, California, Using True- and False-Color Composite Images, Band Ratios, and Logical Operator Algorithms. *Econ. Geol.* **2018**, *113*, 1587–1601. [CrossRef]
15. Perring, C.S. A 3-D Geological and Structural Synthesis of the Leinster Area of the Agnew-Wiluna Belt, Yilgarn Craton, Western Australia, with Special Reference to the Volcanological Setting of Komatiite-Associated Nickel Sulfide Deposits. *Econ. Geol.* **2015**, *110*, 469–503. [CrossRef]
16. Kyne, R.; Torremans, K.; Güven, J.; Doyle, R.; Walsh, J. 3-D Modeling of the Lisheen and Silvermines Deposits, County Tipperary, Ireland: Insights into Structural Controls on the Formation of Irish Zn-Pb Deposits. *Econ. Geol.* **2019**, *114*, 93–116. [CrossRef]
17. Weng, Z.H.; Jowitt, S.M.; Mudd, G.M.; Haque, N. Assessing rare earth element mineral deposit types and links to environmental impacts. *Appl. Earth Sci. IMM Trans. Sect. B* **2013**, *122*, 83–96. [CrossRef]
18. Issayeva, L.D.; Asubaeva, S.K.; Togizov, K.S.; Kembayev, M.K. The formation of a geoinformation system and creation of a digital model of Syrymbet rare-metal deposit (North Kazakhstan). *Int. Multidiscip. Sci. Geo Conf. Surv. Geol. Min. Ecol. Manag. SGEM Bulg.* **2019**, *19*, 609–616. [CrossRef]
19. Laumullin, T.M. Deposits of rare-metals and rare-earths of Kazakhstan. In *Handbook (in Russia)*, 2nd ed.; The Republican State Enterprise on the right of economic management Information and Analytical Centre for Geology and Mineral Resources: Almaty, Kazakhstan, 2015; 270p.
20. Issayeva, L.D.; Togizov, K.S.; Duczmal-Czernikiewicz, A.; Kurmangazhina, M.; Muratkhanov, D. Ore-controlling factors as the basis for singling out the prospective areas within the Syrymbet rare-metal deposit, Northern Kazakhstan. *Min. Miner. Depos.* **2022**, *2*, 14–21. [CrossRef]
21. Rare Earth Element and Rare Metal Inventory of Central Asia. Available online: <https://pubs.usgs.gov/fs/2017/3089/fs20173089.pdf> (accessed on 6 March 2018).
22. Fan, H.-R.; Yang, K.-F.; Hu, F.-F.; Liu, S.; Wang, K.-Y. The giant Bayan Obo REE-Nb-Fe deposit, China: Controversy and ore genesis. *Geosci. Front.* **2016**, *7*, 335–344. [CrossRef]
23. Estrade, G.; Smith, M.P.; Goodenough, K.M.; Nason, P. REE concentration processes in ion adsorption deposits: Evidence from the Ambohimirahavavy alkaline complex in Madagascar. *Ore Geol. Rev.* **2019**, *112*, 1–21. [CrossRef]
24. Zhan, Y.-X.; Li, X.-C.; Wu, B.; Yang, K.-F.; Fan, H.-R.; Li, X.-H. The occurrence and genesis of HREE-rich minerals from the giant Bayan Obo deposit, China. *Ore Geol. Rev.* **2023**, *157*, 105438. [CrossRef]
25. Mohammad, A.M. Rare earth elements geochemistry of recent clastic sediments from different environments from part of the eastern coast of India. *J. Sediment. Environ.* **2021**, *6*, 431–445. [CrossRef]
26. Simandl, G.J. Geology and market dependent significance of rare earth element resources. *Miner. Depos.* **2014**, *49*, 889–904. [CrossRef]
27. Wu, Z.; Chen, Y.; Wang, Y.; Xu, Y.; Lin, Z.; Liang, X.; Cheng, H. Review of rare earth element (REE) adsorption on and desorption from clay minerals: Application to formation and mining of ion-adsorption REE deposits. *Ore Geol. Rev.* **2023**, *157*, 105446. [CrossRef]
28. Bao, Z.W.; Zhao, Z.H. Geochemistry of mineralization with exchangeable REY in the weathering crusts of granitic rocks in South China. *Ore Geol. Rev.* **2008**, *33*, 519–535. [CrossRef]
29. Ichimura, K.; Sanematsu, K.; Kon, Y.; Takagi, T.; Murakami, T. REE redistributions during granite weathering: Implications for Ce anomaly as a proxy for paleoredox states. *Am. Miner.* **2020**, *105*, 848–859. [CrossRef]
30. Dushyantha, N.; Batapola, N.; Ilankoon, I.M.S.K.; Rohitha, S.; Premasiri, R.; Abeysinghe, B.; Ratnayake, N.; Dissanayake, K. The story of rare earth elements (REEs): Occurrences, global distribution, genesis, geology, mineralogy and global production. *Ore Geol. Rev.* **2020**, *122*, 103521. [CrossRef]

Disclaimer/Publisher’s Note: The statements, opinions and data contained in all publications are solely those of the individual author(s) and contributor(s) and not of MDPI and/or the editor(s). MDPI and/or the editor(s) disclaim responsibility for any injury to people or property resulting from any ideas, methods, instructions or products referred to in the content.